Master's Thesis

Pyrolysis Effect on the Stabilization Characteristics of Autoignited Dimethyl Ether Jet Flames in Heated Coflow Air

BAREUM JUNG

Department of Mechanical Engineering

Graduate School of UNIST

2019

Pyrolysis Effect on the Stabilization Characteristics of Autoignited Dimethyl Ether Jet Flames in Heated Coflow Air

BAREUM JUNG

Department of Mechanical Engineering

Graduate School of UNIST

Pyrolysis Effect on the Stabilization Characteristics of Autoignited Dimethyl Ether Jet Flames in Heated Coflow Air

A thesis/dissertation
submitted to the Graduate School of UNIST
in partial fulfillment of the
requirements for the degree of
Master of Science

BAREUM JUNG

December/12/2018
Approved by

_____

Advisor
Chun Sang Yoo

Pyrolysis Effect on the Stabilization Characteristics of Autoignited Dimethyl Ether Jet Flames in Heated Coflow Air

BAREUM JUNG

This certifies that the thesis/dissertation of Ba Reum Jung is approved.

December/12/2018

Signature

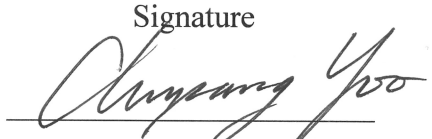

Advisor: Chun Sang Yoo

Signature

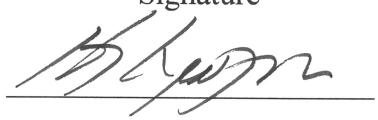

Hyungson Ki

Signature

Jaesung Jang

Abstract

The stabilization characteristics of autoignited laminar dimethyl ether (DME) jet flames in heated coflow air are numerically investigated with laminarSMOKE code, which is an OpenFOAM-based laminar reacting flow solver. According to a previous experiment on autoignited laminar DME jet flame, an unusual liftoff height behavior is observed such that liftoff height of lifted flame decreases with increasing fuel jet velocity. To understand the liftoff and ignition characteristics of autoignited DME jet flames, various numerical studies have been carried out in the present paper. From a series of numerical studies, it is elucidated that the decreasing liftoff height behavior is mainly due to the autoignition of DME such that liftoff height variations can be well correlated to ignition delay time. Due to the high mass diffusive characteristic of hydrogen molecule, the more amount of hydrogen molecule is diffused out from the flame region as fuel jet velocity decreases, leading to the difference between liftoff height and ignition delay time. To verify whether or not the decreasing liftoff height trend is general behavior, additional simulation is conducted by varying fuel nozzle length from 0.75 to 3 m. All the results consistently show decreasing liftoff height with the increase of fuel jet velocity for a relatively-low fuel velocity regime. However, there is no specific correlation between nozzle length and liftoff height, which would be attributed to the non-monotonous ignition delay time variations with the different levels of pyrolysis. According to the results from sensitivity analysis and pseudo CH_2O model, it is demonstrated that the different amount of CH_2O mainly controls the non-monotonous ignition delay time. Last, the pyrolysis effect on the ignition and liftoff height characteristics of autoignited laminar DME jet flame is investigated by varying the fuel nozzle length while the fuel jet velocity is fixed to 5 m/s. Various types of flames can be observed depending on the degree of pyrolysis such as the MILD combustion, transition, tribrachial edge flame, and attached flame. In the MILD combustion regime where the pyrolysis effects are relatively-less dominant to the flame, the liftoff height variations are well correlated with the variations of 0-D ignition delay. In transition and tribrachial edge flame regimes, however, the liftoff height trend is no longer to be consistent with ignition delay time. From Chemical Explosive Mode Analysis (CEMA), it is found that the distinct autoignition characteristics depend on the degree of the fuel pyrolysis.

Keywords: Autoignition, ignition delay, liftoff height, MILD combustion, CEMA

Contents

List of Figures

List of Tables

1. Introduction

Dimethyl ether (DME) is the simplest ether with the formula of CH_3OCH_3, simplified to C_2H_6O as shown in Fig. 1. DME can be produced from natural gas or coal gasification process. Due to the short carbon chain in DME, the emission of particulate matters remains very low during its combustion process [1]. Also, DME can be used as an ignition improver because of its low autoignition temperature (~ 508 K) compared to those of other hydrocarbon fuels [2, 3, 4, 5, 6, 7].

It is of importance to note that DME is easily decomposed into methane (CH_4), hydrogen (H_2), formaldehyde (CH_2O) and etc. under inert atmosphere at high temperatures. Such pyrolysis of DME plays a critical role in changing its flame characteristics such as ignition delay time, lift-off height, and flame temperature. Because of this importance, flow reactor and shock tube experiments have been carried out to accurately measure the pyrolysis, and kinetic mechanism haven been developed through sensitivity analysis for numerical analysis [8]. The characteristics of the pyrolysis should be preceded for better understanding of the flame characteristics.

An autoignition process of fuel jets in heated air has received great attention during the past several decades because it is widely observed in various practical engines such as a gas turbine or a diesel engine. Many researchers have been involved to understand the fundamental characteristics of the autoignition process. The autoignition characteristics of laminar lifted flames have been investigated both experimentally and numerically [9, 10, 11, 12, 13, 14, 15], and the results showed that an autoignited laminar non-premixed fuel jet develops into a stationary lifted flame or a nozzle-attached flame depending on the initial conditions of the fuel and coflow air jets. The autoignited lifted flames are found to be stabilized regardless of the Schmidt number (Sc) [10], while the non-autoignited lifted flames can be stabilized only if Sc is greater than unity [16, 17].

The autoignited lifted jet flames stabilize in the form of a tribrachial edge, or moderate or intense low-oxygen dilution (MILD) combustion; the lifted flame with the tribrachial edge develops when the initial fuel mole fraction in fuel jet ($X_{F,0}$) is relatively high while the MILD combustion appears when

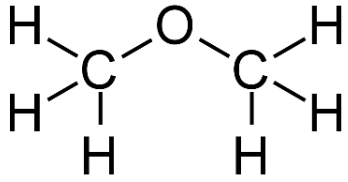

Figure 1. The molecular structure of dimethyl ether

$X_{F,0}$ is considerably low. For the tribrachial edge flame, its leading edge consists of lean/rich premixed flame wings and a trailing diffusion flame along the stoichiometric mixture fraction isoline [15] as shown in Fig. 2. When the fuel jet is largely diluted with nitrogen, the typical tribrachial edge flame is not observed and its flame structure changes to the MILD combustion.

The liftoff height of laminar lifted flames is generally proportional to the fuel jet velocity, provided that all the other conditions remain the same. The correlation between the fuel jet velocity and liftoff height has been devised as $H_L \sim U_0 t^2_{ig,ad}$, where H_L is the liftoff height, U_0 the jet velocity, and $t_{ig,ad}$ the 0-D adiabatic ignition delay time at the stoichiometric condition based on the fuel and oxidizer mixtures [9, 11]. It is found that the correlation can capture the behaviors of various types of single component fuel jet flames with the tribrachial edge. For the autoignited lifted flames with the MILD combustion, H_L is found to be correlated with $H_L \sim U_0 Y_{F,0} t^2_{ig,ad}$, where $Y_{F,0}$ is the initial mass fraction of the fuel representing the fuel strength [10]. For both H_L correlations, H_L is dependent on $t^2_{ig,ad}$, which implies that the adiabatic ignition delay time plays an important role in stabilizing the autoignited lifted flames.

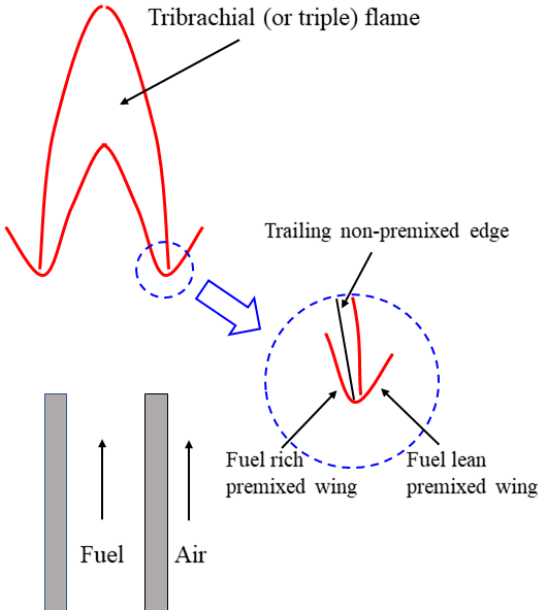

Figure 2. Schematic of a laminar lifted tribrachial edge flame.

However, from an experimental study of autoignited laminar lifted DME jet flames in heated coflow air, an unusual H_L behavior was observed; H_L is inversely proportional to the fuel jet velocity, U_0 [18]. In general, this decreasing H_L behavior occurs only when two kinds of fuels are mixed in the fuel jet (e.g., methane/hydrogen jet flames) [19], and the differential diffusion effect between the two fuels is found to determine the unusual liftoff height behavior. DME is a single component fuel such that the differential diffusion effect can be neglected. However, DME can be easily decomposed into smaller species such as CH_4 and H_2 at high temperatures through a heated fuel nozzle and hence, the decreasing H_L behavior of DME jet would be also attributed to the differential diffusion effect but its detailed reasons remain unclear [18]. Additionally, the ignition delay time would also affect the unusual H_L behavior because it is significantly varied by the degree of pyrolysis in the DME jet.

Therefore, the objective of the present paper is to investigate the combustion characteristics of autoignited laminar lifted DME jet flames by performing two-dimensional detailed numerical simulations. More specifically, we elucidate the reason why the unusual H_L behavior occurs with increasing U_0 and the different autoignition mechanism of the lifted flames depending on the degree of the DME pyrolysis.

.

2. Numerical methods

The present numerical simulations were performed in a two-dimensional axisymmetric coordinate in the radial, *r*- and the axial, *z*-, directions. The domain size is 6.65 cm × 50 cm in the *r*- and *z*-directions, respectively, which is identical to that of experiments [10]. The inner radius of the fuel jet is 0.188 cm, and the fuel jet nozzle thickness is 0.05 cm. In the *r*- direction, 100 μm mesh size is uniformly distributed within 1.5 cm, and stretched mesh is applied to the remaining area while the uniform 100 μm mesh size is used in the *z*- direction. A schematic configuration for the present simulation domain is shown in Figure 3.

A grid convergence test was carried out for a case with L_{res} = 0.75 m (the length of fuel nozzle at inlet), T_0 = 980 K (coflow & wall temperature), T_C = 300 K (inlet temperature), and U_0 = 5 m/s with different mesh sizes of 50, 100, and 200 μm. Figure 4 show that there is no apparent discrepancy between the results of the current mesh size of 100 μm and the finer mesh size of 50 μm. Therefore, we believe that the current mesh size of 100 μm is fine enough to elucidate the combustion characteristics of the present study.

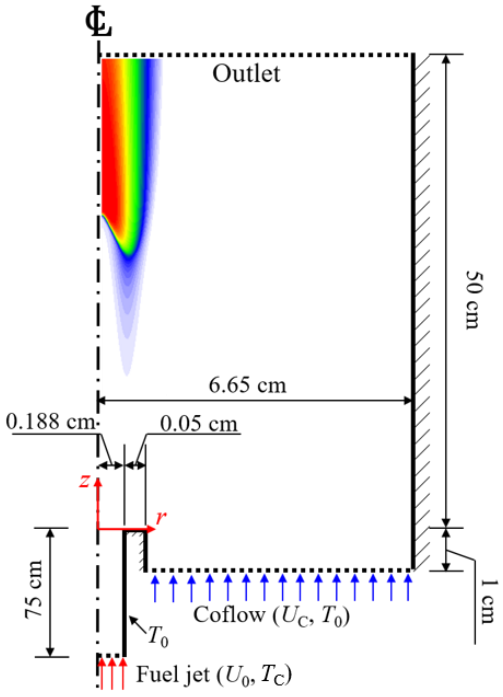

Figure 3. Schematic of the computational configuration for the present simulations of autoignited laminar lifted DME jet flames in heated coflow.

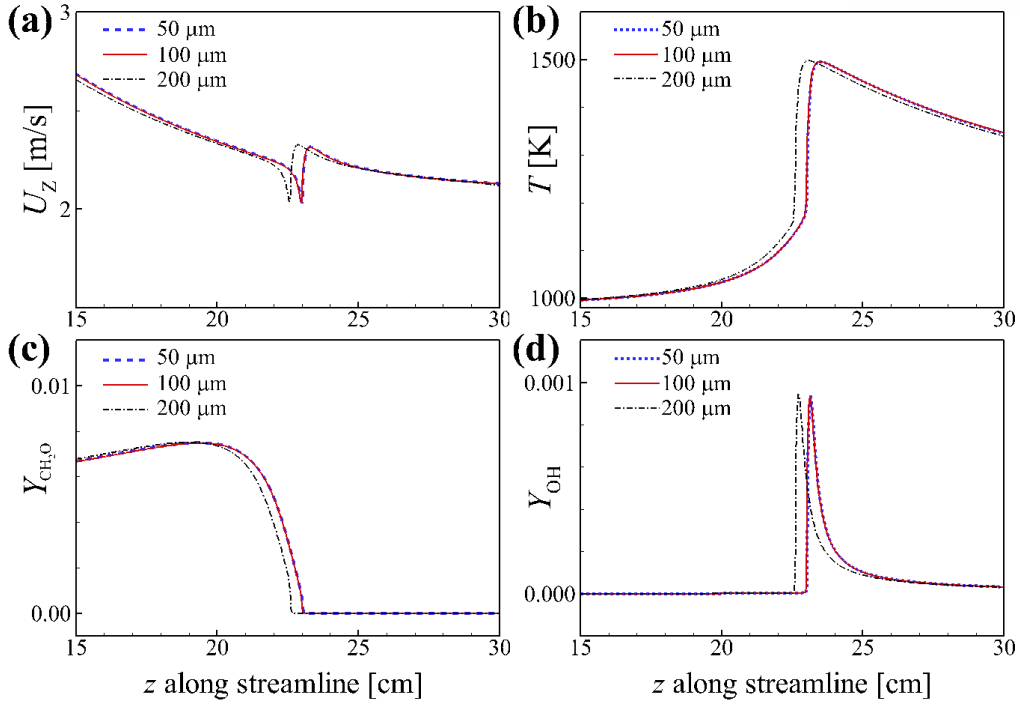

Figure 4. Profiles of (a) axial velocity, (b) temperature, mass fractions of (c) CH_2O and (d) OH of a lifted DME jet flame along the streamline for three different grid resolutions. The inlet velocity and fuel nozzle length of the fuel jet are U_0 = 5 m/s and L_{res} = 0.75 m, respectively.

The present numerical simulations were performed using the laminarSMOKE code, which is an OpenFOAM [20] based numerical framework for simulations of compressible laminar reacting flows in multi-dimensional geometries with a detailed chemical kinetic mechanism. The laminarSMOKE code solves the conservation equations of mass, momentum, species, and energy:

$$\nabla(\rho\mathbf{v}) = 0,$$

$$\nabla(\rho\mathbf{v}\mathbf{v} + p\mathbf{I}) = \nabla\boldsymbol{\tau} + \rho\mathbf{g},$$

$$\nabla(\rho Y_i\mathbf{v}) = -\nabla(\rho Y_i\boldsymbol{V_i}) + \dot{\Omega}_i,$$

$$\rho C_p\mathbf{v}\nabla T = -\nabla\mathbf{q} - \rho\sum_{i=1}^{NC} C_{p,i}Y_i\boldsymbol{V_i} - \sum_{i=1}^{NC} h_i\dot{\Omega}_i,$$

where ρ is the density, $\mathbf{v}$ the gas mixture velocity, $\boldsymbol{\tau}$ the stress tensor, $\mathbf{g}$ the gravity vector, Y_i the mass fraction of species i, $\boldsymbol{V_i}$ the diffusion velocity of species i, $\dot{\Omega}_i$ the net production rate of species i, C_p the specific heat of mixture at constant pressure, $\mathbf{q}$ the heat flux, and h_i the local enthalpy of species i.

Stress tensor $\boldsymbol{\tau}$:

$$\boldsymbol{\tau} = \left[p + \left(\frac{2}{3}\mu - \kappa\right)(\nabla \cdot \mathbf{v})\right]\mathbf{U} - \mu[(\nabla \mathbf{v}) + (\nabla \mathbf{v})^T],$$

where $\mathbf{U}$ is the unit tensor, μ the dynamic viscosity, κ the second coefficient of viscosity, and the superscript T denotes transpose of the tensor.

Diffusion velocities $\mathbf{V}_i$:

$$\mathbf{V}_i = -\frac{\Gamma_i}{Y_i}\nabla Y_i - \frac{\Gamma_i \Theta_i}{X_i}\frac{1}{T}\nabla T,$$

where Γ_i is the individual species mixture averaged diffusion coefficient, X_i the mole fraction and Θ_i the thermal diffusion ratio of species of i.

Net production rate of species i $\dot{\Omega}_i$:

$$\dot{\Omega}_i = W_i \sum_{k=1}^{K} (v''_{i,k} - v'_{i,k}) B_k T^{\alpha_k} \exp(-E_{a,k}/R^{\circ}T) \prod_{j=1}^{N} c_j^{v'_{j,k}}, \qquad i = 1, \ldots, N,$$

where $v''_{i,k}$ and $v'_{i,k}$ is the corresponding i-th species molar concentration coefficient of product and reactant of k-th reaction, respectively. W_i the molecular weight. B_k is the constant of k-th reaction, α the temperature exponent, E_a the activation energy, and $c_j = \rho_j / W_j$.

Heat flux **q:**

$$\mathbf{q} = -\lambda \nabla T + \mathbf{q}_{rad},$$
$$\mathbf{q}_{rad} = -4\sigma a_P (T^4 - T_{env}^4),$$

where λ is the mixture thermal conductivity, σ the Stefan-Boltzmann constant and T_{env} the environment temperature. The plank mean absorption coefficient a_P is evaluated according to the following expression:

$$a_P = p_{\mathrm{H_2O}} a_{p,\mathrm{H_2O}} + p_{\mathrm{CO_2}} a_{p,\mathrm{CO_2}} + p_{\mathrm{CO}} a_{p,\mathrm{CO}} + p_{\mathrm{CH_4}} a_{p,\mathrm{CH_4}},$$

where p_k is the partial pressure of species k. The extinction coefficient $a_{p,k}$ of species k is derived from calculations performed by the RADCAL software [21].

The mass and momentum conservation equations are solved by SIMPLE algorithm in the steady the laminarSMOKE solver, and transport and reaction terms are decoupled in the species and energy conservation equation to resolve the stiffness issue between the transport and reaction terms. For more information about the solver, readers are referred to [22, 23]. A detailed 53-species of DME/air chemical kinetic mechanism [24] is adopted for the present simulations.

All the boundary conditions are consistent with the experimental conditions. Uniform pipe flow condition is applied for the fuel jet inlet with the flow velocity of U_0, and coflow velocity, U_C, is fixed

to be 1.1 m/s. Fixed value of temperature is specified for fuel (T_C) and air inlets (T_0) as 300 and 980 K, respectively. The DME fuel is heated up to 980 K as it passes through the fuel jet nozzle with 980 K. Except for the fuel nozzle wall, adiabatic boundary conditions are applied for the other wall boundaries. No slip boundary conditions are applied for all the wall boundaries and the symmetric boundary condition is used for the centerline. For the outlet, zero-gradient outflow boundary conditions are used. Pressure boundary condition at the inlet and the outlet are zero-gradient and atmospheric, respectively. The DME fuel jet is diluted with nitrogen such that the fuel mole fraction at the inlet, $X_{F,0}$, is 0.08.

3. Characteristic of lifted flame under an experimental condition

In the previous experiments of the DME lifted jet flames [18], the decreasing H_L behavior with increasing U_0 (i.e., $H_L \sim 1/U_0$) was observed when T_0 is 860 ~ 900 K, $X_{F,0}$ is 0.036 ~ 0.160, and L_{res} is 0.75 m. On the other hand, H_L was found to be proportional to U_0 (i.e., $H_L \sim U_0$) when $X_{F,0}$ is 0.14 ~ 0.26. It is noted that T_0 in the present simulations are greater than those in experiments [24], which is probably attributed to uncertainties in the chemical mechanism and transport data and/or experiments. This issue has been also reported in the previous numerical studies [26, 28].

3.1. Unusual liftoff height behavior ($H_L \sim 1/U_0$)

First, we capture the unusual liftoff height behavior of the DME jet flames at T_0 = 980 K, U_0 = 1.5 ~ 6 m/s, $X_{F,0}$ = 0.08, and L_{res} = 0.75 m using laminarSMOKE. Figure 5 shows H_L and T_{max} as a function of U_0. Figure 6 shows the iso-contours of temperature and mass fraction of OH (Y_{OH}) for the DME jet flames. The liftoff height H_L is the z-directional length between the fuel nozzle rim and the flamebase. To precisely measure the liftoff height, we adopt the chemical explosive mode analysis (CEMA) and determine the flamebase as the most upstream location of $\mathrm{Re}(\lambda_{exp}) = 0$ isoline, where λ_{exp} is an eigenvalue of the Jacobian of the chemical source term [25, 26, 27, 28, 29, 30]. Note that mixtures with $\mathrm{Re}(\lambda_{exp}) > 0$ means that they are self-ignitable, whereas mixtures with $\mathrm{Re}(\lambda_{exp}) < 0$ is ignited or non-ignitable. Therefore, the isoline of $\lambda_{exp} = 0$ denotes the boundary between the non-explosive and explosive regions, and hence, it can be used to distinguish burned and unburnt regions.

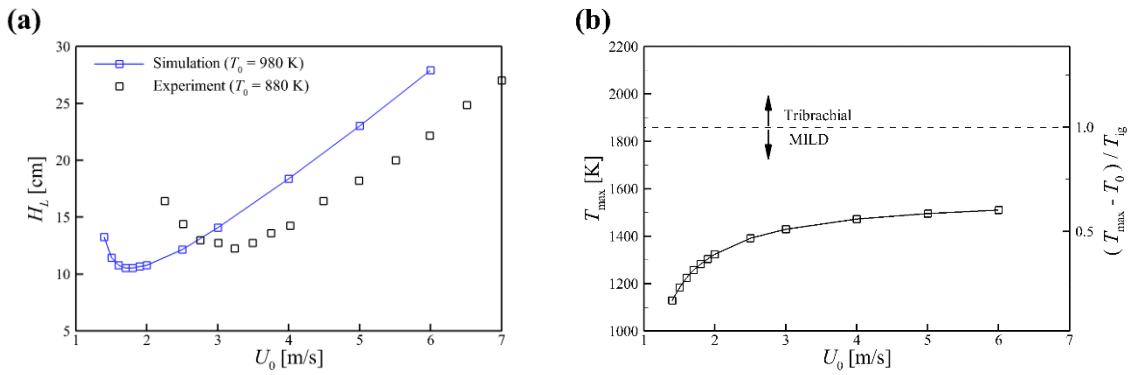

Figure 5. Variation of (a) H_L and (b) T_{max} for different U_0 under $X_{F,0}$ = 0.08 and T_0 = 980 K condition. H_L of the experiment (black square symbol) is also shown as a reference

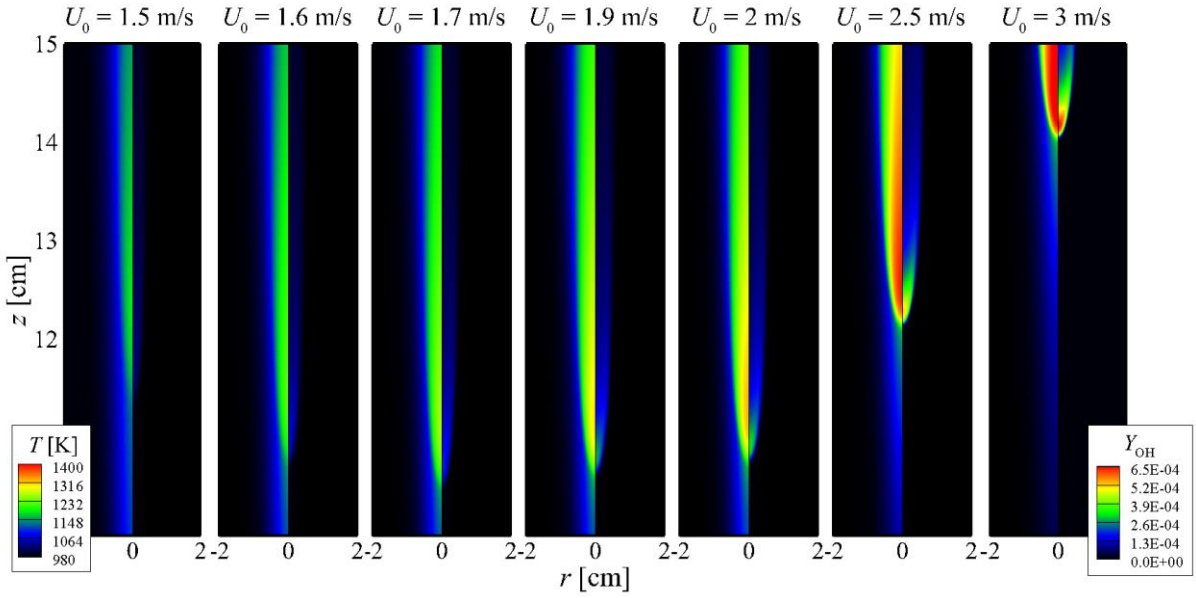

Figure 6. Isocontours of (a) T (right half), and mass fraction of OH (left half) for autoignited laminar lifted DME jet flames for U_0 = 1.5 ~ 3 m/s.

For comparison purpose, Fig. 5 shows the H_L variations from experimental results [18]. The decreasing and increasing liftoff height behavior with increasing U_0 ("U-shaped" behavior) is qualitatively captured in the present simulations. However, there is slight difference in U_0 at which the lowest height appears. The simulation result shows that the lowest liftoff height appears at lower jet velocity. This difference is probably attributed to the imperfect kinetic mechanism of DME oxidation. Although there are some discrepancies, the present simulation results well capture non-monotonic H_L behavior.

To categorize the distinct combustion feature of the lifted flames [9, 31, 32], we measure $(T_{max}-T_0)$ / T_{ig} as shown in Fig. 5b. In principle, the MILD combustion occurs when $(T_{max}-T_0)$ / $T_{ig} > 1$, and the tribrachial edge flame occurs when $(T_{max}-T_0)$ / $T_{ig} < 1$ and $T_0 > T_{ig}$ are both satisfied [9, 15, 32]. T_{ig} is the minimum temperature for autoignition of the stoichiometric mixture based on the inlet conditions. We determine T_{ig} considering that autoignition can occur within the computational domain if 0-D ignition delay time, τ_{ig}^0, at $T = T_{ig}$ is less than one-jet flow-through time of the coflow air. Note that τ_{ig}^0 is evaluated using CHEMKIN software [33]. As shown in Fig. 5b, all the flames under this condition are categorized into the MILD combustion regime, which implies that τ_{ig}^0 would dominantly affect the stabilization of the lifted flame [19].

3.2. 0-D simulation about DME's pyrolysis

As mentioned above, Al-Noman et al. [18] conjectured that the unusual decreasing H_L behavior with increasing U_0 would be attributed to the disparity between the mass diffusivities of hydrogen and other species or ignition delay times which are dependent on the degree of pyrolysis. To better understand the pyrolysis of the DME fuel jet through the fuel nozzle, 0-D simulations were carried out. Figure 7 shows the generation/consumptions of major species and the resultant τ_{ig}^0 variation with increasing residence time using CHEMKIN software [33]. The initial conditions are same as the previous 2-D conditions (i.e., T_0 = 980 K, $X_{F,0}$ = 0.08, and p = 1 atm).

It is readily observed from Fig. 7 that the longer the residence time is, the more CH_4 and H_2 are produced. That is, as L_{res} becomes longer, the pyrolysis of the DME jet is enhanced and as such, more CH_4 and H_2 are injected from the nozzle. In addition, several points are to be noted from the Fig. 7. τ_{ig}^0 first decreases and then increases when the mole fraction of CH_2O is relatively large in Regime I. This result implies that τ_{ig}^0 would be highly influenced by the amount of CH_2O, X_{CH_2O}, which is known as an ignition improver [5-10]. In Regime II, on the other hand, τ_{ig}^0 decreases with decreasing X_{CH_2O}, which implies that CH_2O does not affect τ_{ig}^0, or CH_2O becomes an ignition retarder.

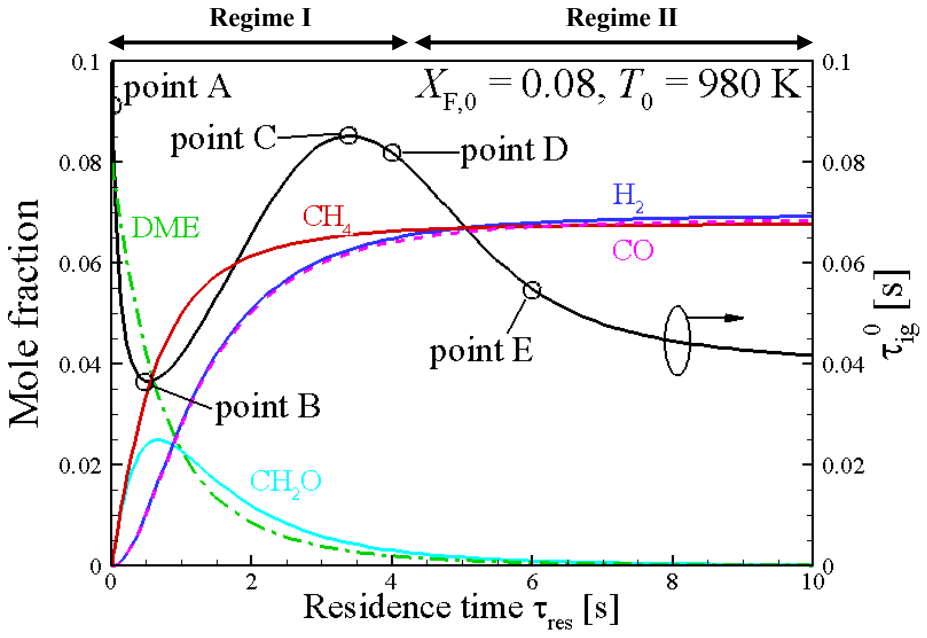

Figure 7. Mole fraction and ignition delay time with residence time at $X_{F,0}$ = 0.08, p = 1 atm, and T_0 = 980 K from the 0-D homogeneous simulation

To understand the fundamental role of CH_2O in both regimes, a pseudo-CH_2O model and sensitivity analysis were carried out. First, the pseudo-CH_2O analysis was performed by replacing CH_2O in the fuel mixture into a pseudo-CH_2O of which thermodynamic properties are the same as those of real CH_2O while it does not participate in the reactions. The results are shown in Fig. 8. In Regime I, τ_{ig}^0 with the pseudo CH_2O model becomes longer than that for the normal case, which denotes that CH_2O plays the fundamental role in advancing τ_{ig}^0. In Regime II, however, τ_{ig}^0 for the pseudo-CH_2O model is slightly shorter than that for the normal case. Therefore, it is reasonable to consider that CH_2O in Regime II retards the overall 0-D ignition. In addition, DME is almost diminished due to the pyrolysis such that we can assume that overall 0-D ignition characteristics and the role of CH_2O are different in these two regimes.

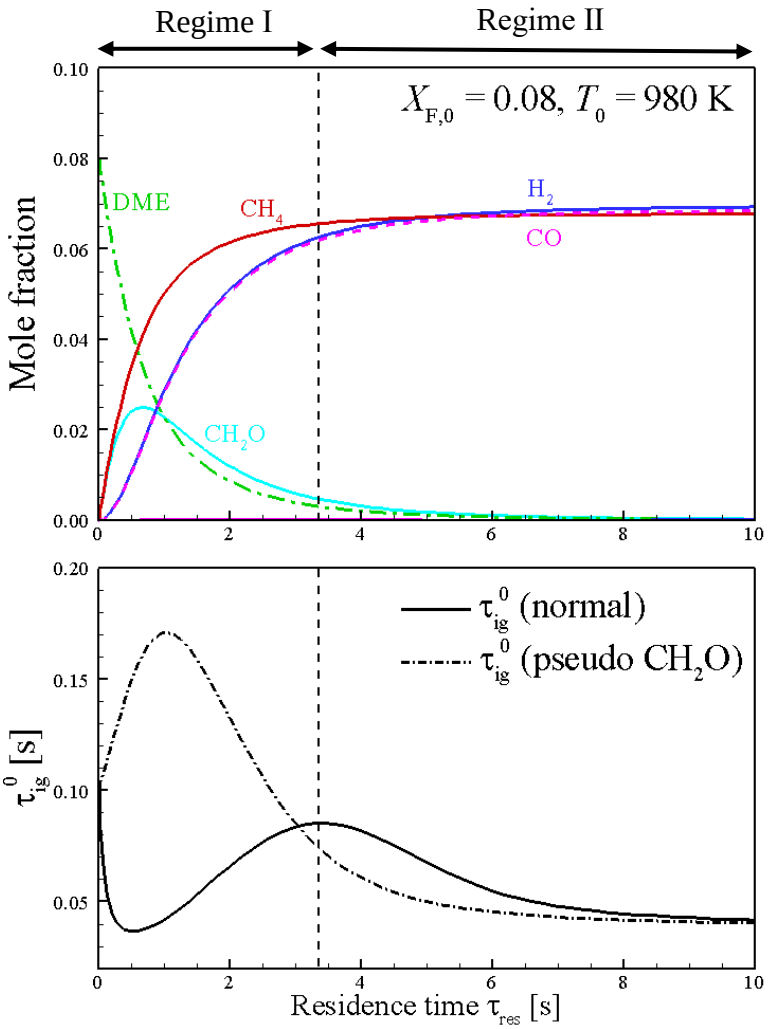

Figure 8. 0-D ignition delay time calculation depending on the different pyrolysis stage of DME using normal (black solid line) and pseudo (black dash dot line) CH_2O.

To investigate the detailed role of CH_2O for both regimes, the sensitivity analysis was carried out on several representative points from A to E in Fig. 7. The results are shown in Fig. 9. Sensitivity coefficient (SC) is the changing ratio of τ_{ig}^0 by doubling the rate constant of *i*-th reaction, k_i. Therefore, negative value of SC for *i*-th reaction denotes that this reaction reduces τ_{ig}^0 and vice versa.

In Regime I (from point A to C), τ_{ig}^0 variation is well correlated with $CH_2O + HO_2 \rightarrow HCO + H_2O_2$ (R42) and $H_2O_2 + M \rightarrow OH + OH + M$ (R16). CH_2O reacts primarily with HO_2 that is generated by the pyrolysis of DME through R42, generating H_2O_2. H_2O_2 is subsequently decomposed into OH via R16, which is one of the exothermic reactions of hydrocarbon. Therefore, more CH_2O in Regime I can enhance R16, leading to the reduction of τ_{ig}^0. In Regime II (from point C to E), however, the hydrogen chain branching reaction, $H + O_2 \rightarrow O + OH$ (R1), becomes dominant while the initiation of DME pyrolysis, $CH_3OCH_3 + CH_3 \rightarrow CH_3OCH_2 + CH_4$ (R134), becomes negligible as compared to that in Regime I. It is also of interest to note that CH_2O is mainly involved in $CH_2O + H \rightarrow HCO + H_2$ (R38) rather than R42 such that CH_2O plays a negative role in autoignition. Since the overall ignition characteristics in Regime II follows hydrogen ignition more than DME ignition, CH_2O can be considered as an ignition retarder. In summary, we can divide the ignition characteristics of DME fuel into Regimes I and II based on different ignition characteristics; DME ignition is dominant at relatively-low pyrolysis stage (Regime I) and the overall ignition characteristics change to that of hydrogen ignition at relatively-high pyrolysis stage (Regime II).

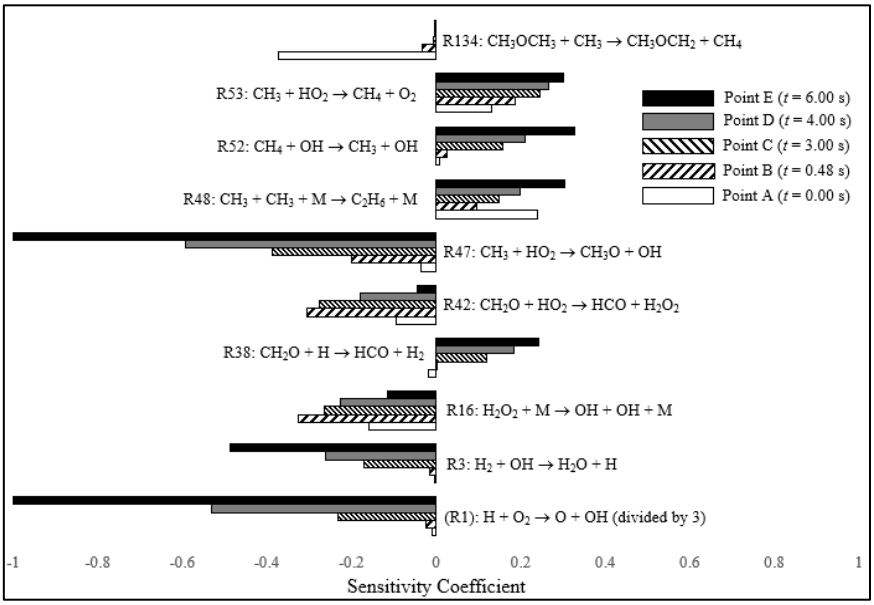

Figure 9. Sensitivity analysis depending on the different pyrolysis stage of DME (from point A to E)

3.3. Correlation between ignition delay time and H_L

As mentioned above, the unusual decreasing H_L behavior with increasing U_0 would be attributed to τ_{ig}^0, which is dependent on the degree of pyrolysis. This hypothesis is based on an observation that H_L shows decreasing behavior following τ_{ig}^0. To verify whether τ_{ig}^0 induces the unusual decreasing H_L tendency or not, we plot H_L with τ_{ig}^0 in Fig. 10, where U_0 is defined in 0-D domain as $U_0 = 0.75/\tau_{res}$. As shown at Fig.10, the overall behavior of H_L follows τ_{ig}^0. However, there is a slight difference between H_L and τ_{ig}^0 trends as U_0 decreases. This is probably because CH_4 and H_2 from the DME pyrolysis increase the inhomogeneity of ignition that contributes to differentiating H_L from τ_{ig}^0 trend. To verify this, additional 2-D simulations were carried out.

Additional numerical simulations were performed by artificially changing the mass diffusivity of the hydrogen molecule, D_{H_2}, to that of DME. Figure 11 shows results of the simulation. The blue solid line represents the cases with modified D_{H_2}. It is readily observed from the Fig. 11 that H_L with the modified D_{H_2} follow τ_{ig}^0 trend very well. From these results, we can conjecture that the large D_{H_2} causes the difference between H_L and τ_{ig}^0. In addition, the U-shaped behavior of H_L is irrelevant to the D_{H_2} because the U-shaped behavior always appears whatever the value of D_{H_2} is. Therefore, it can be summarized that due to the pyrolysis process of the DME jet through the fuel nozzle, relatively-large amount of H_2 is generated at relatively-lower U_0 condition, which ultimately affects the difference between H_L and τ_{ig}^0 due to the high mass diffusivity of hydrogen molecule. However, it does not change the U-shaped behavior of the liftoff height.

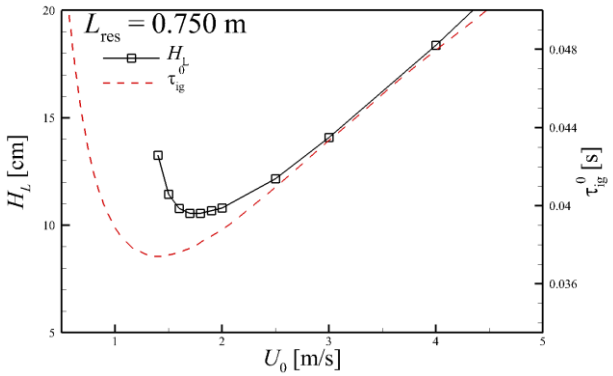

Figure 10. Variation of H_L (black solid line) and τ_{ig}^0 (red dot line) for different U_0 under $X_{F,0}$ = 0.08 and T_0 = 980 K condition.

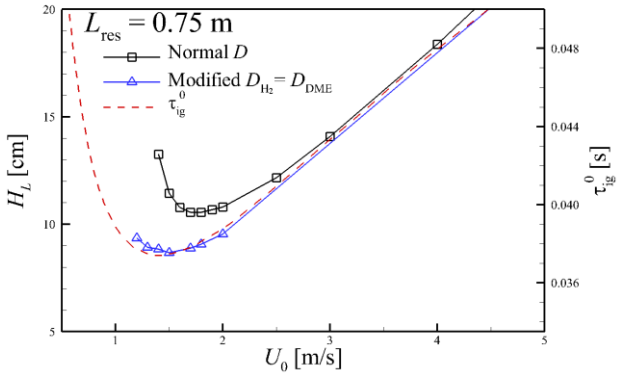

Figure 11. The variation of H_L for various fuel jet velocities with normal and modified H_2 diffusivity.

3.4. Ignition Characteristics in 2-D jet flame: CEMA

To investigate the different ignition characteristics of the lifted DME jet flames with various pyrolysis level and flame structures, we performed the CEMA for several cases. In the CEMA, the contribution of an *i*-th species to a chemical explosive mode (CEM) is defined as an explosive index, EI, and the contribution of *k*-th reaction to a CEM is defined as a participation index, PI. All the values of EI and PI are normalized between 0 and 1 as follows:

$$\mathbf{EI} = \frac{diag|\mathbf{a}_e\mathbf{b}_e|}{sum(diag|(\mathbf{a}_e\mathbf{b}_e)|)},$$

$$\mathbf{PI} = \frac{(\mathbf{b}_e \cdot \mathbf{S}) \otimes \mathbf{R}}{sum(|(\mathbf{b}_e \cdot \mathbf{S}) \otimes \mathbf{R}|)},$$

where $\mathbf{a}_e$ is the right eigenvector, $\mathbf{b}_e$ the left eigenvector, $\otimes$ the symbol of element-wise multiplication of two vectors, **S** the stoichiometric coefficient matrix, and **R** the vector of net rates for the reactions. Thus, a large value of *i*-th EI and *k*-th PI indicate that *i*-th species and *k*-th reactions are dominant for the CEM, respectively. For more details of the CEMA, readers are referred to [27, 28, 29, 30].

Figure 12 shows the isocontours of EI for several important species in three kind of regimes (i.e., U_0 = 1.5, 1.9, and 5m/s cases which represent the lowest U_0, lowest H_L, and high U_0 regimes, respectively). The white dashed line in the figure denotes the flame region defined by Re(λ_{exp}) = 0. Several points are noted from Fig. 12. First, even though EI's of all species become important to the CEM at different locations, they have similar trends for all regimes. This implies that all flames have similar flame stabilization mechanism. EI's of HO_2 and H_2O_2 (Figs. 12d and 12e), which is related with the DME ignition as shown in 0-D calculations, are already finished upstream of the flamebase and then they

affect thermal ignition (Fig. 12c) for all cases.

To further investigate the different ignition characteristics for each case, especially for chemical reactions, isocontours of PI's for several key reactions are shown in Fig. 13: chain branching reaction of hydrogen, $H + O_2 \rightarrow O + OH$ (R1), the main heat release reaction of hydrogen, $H_2 + OH \rightarrow H + H_2O$ (R3), and HO_2 formulation step, $H + O_2 + M \rightarrow HO_2 + M$ (R9), respectively. Figures 13d, 13e, and 13f show the isocontours for DME related reactions. For all cases, hydrogen-related reactions do not affect the upstream of the flamebase. Rather, these reactions are already diffused out from the flame region. Instead, DME-related reactions are activated upstream of the flamebase in the following sequence: after H-abstraction reactions of DME (Fig. 13d), $CH_3OCH_3 + OH$ (H, O, HO_2, O_2) $\rightarrow$ $CH_3OCH_2 + H_2O$ (H_2, OH, H_2O_2, HO_2), the important exothermic reaction of hydrocarbon (Fig. 13f), $H_2O_2 + M \rightarrow OH + OH + M$ (R16), subsequently occurs near the flame region. Therefore, the autoignition characteristics of lifted flame follow the ignition of DME such that H_L variations can be well correlated to τ_{ig}^0 and unusual H_L behavior can be explained by the ignition of DME.

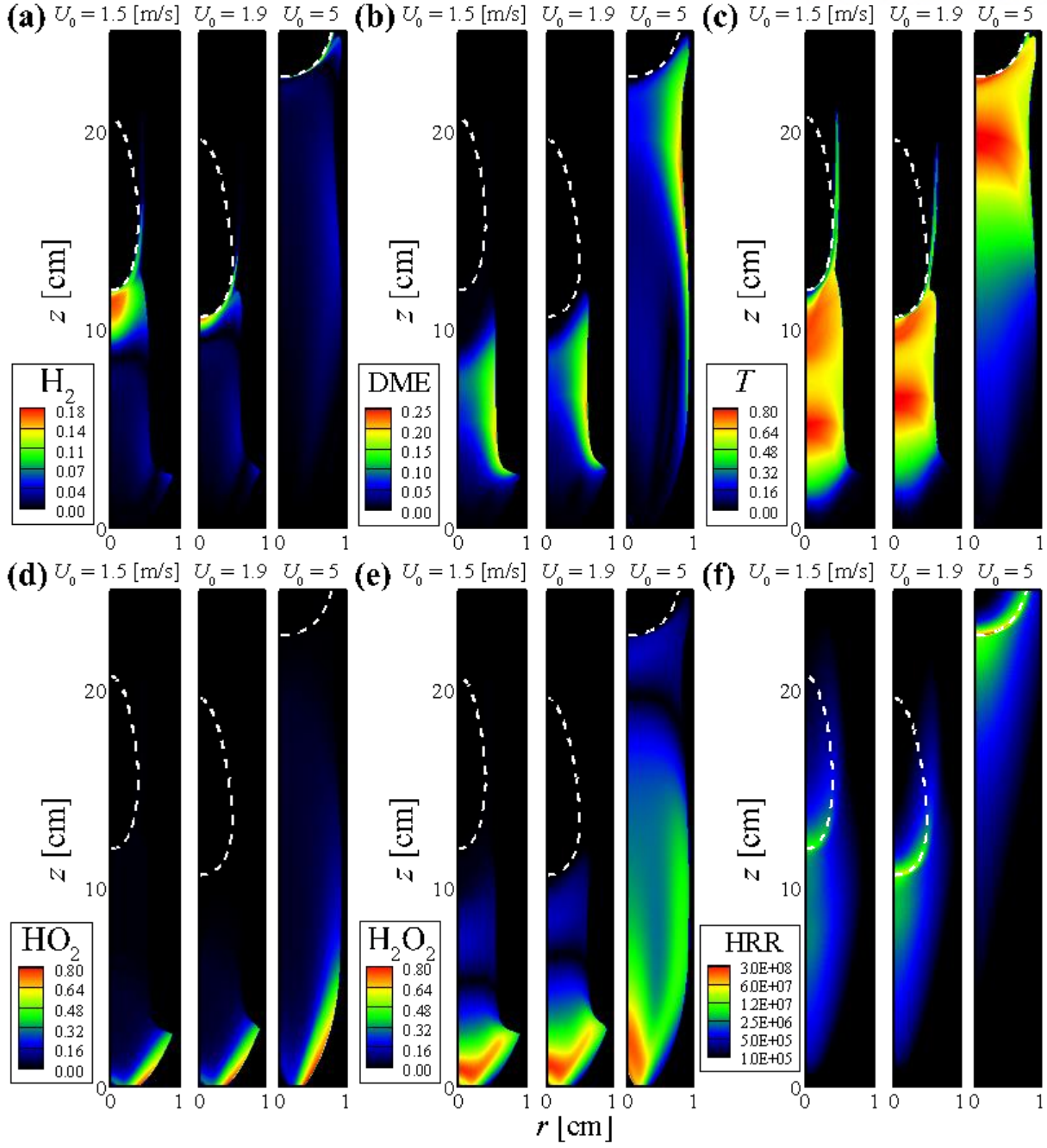

Figure 12. Isocontours of EI of (a) H_2, (b) CH_4, (c) T, (d) HO_2, (e) H_2O_2, and (f) DME for autoignited laminar lifted DME jet flames with different velocities, U_0 = 1.5, 1.9, 5 m/s cases. The white dashed line represents an isoline of Re(λ_{exp}) = 0.

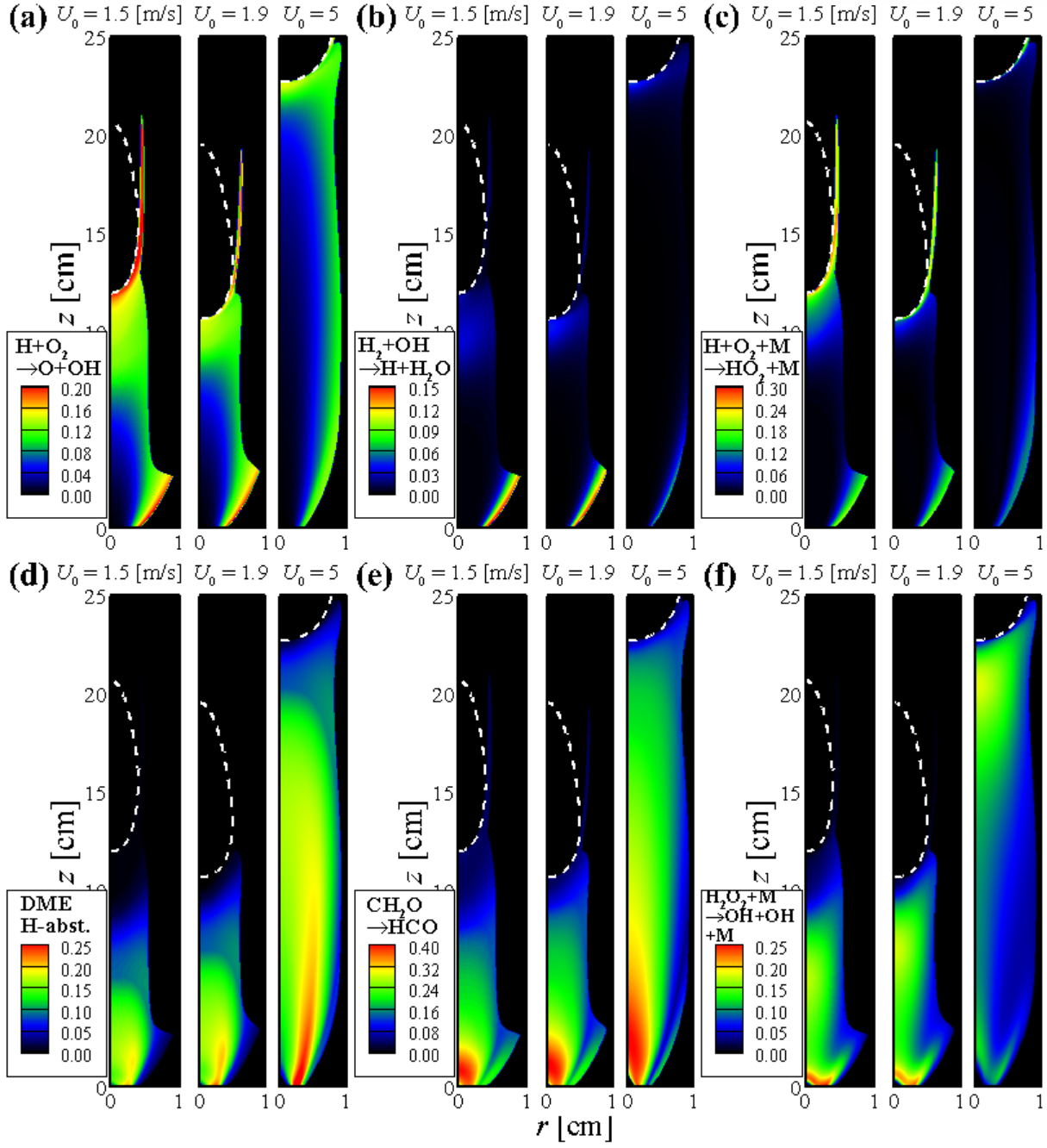

Figure 13. Isocontours of PI of (a) chain branching reaction of hydrogen, (b) heat release step of hydrogen, (c) HO_2 formulation, (d) DME H-abstraction, (e) CH_2O to HCO reactions, and (f) heat release step of hydrocarbon for autoignited laminar lifted DME jet flames with different velocities, U_0 = 1.5, 1.9, 5 m/s cases. The white dashed line represents an isoline of Re(λ_{exp}) = 0.

4. Pyrolysis effects

In this section, we examine how the pyrolysis of DME jet through the fuel nozzle affects flame characteristics. First, we verify whether the "U-shaped" H_L behavior is consistent with the variations of L_{res}. Second, we investigate the effects of the pyrolysis on H_L and autoignition characteristics of the DME jet flame by adjusting L_{res} with fixed U_0 of 5 m/s. Boundary conditions for the present parametric studies are summarized in Table 1 and 2.

Nozzle length L_{res} [m]	Fuel inlet velocity U_0 [m/s]
0.75	1.5 ~ 6
1.5	1.75 ~ 6
3	2.25 ~ 6

Table1. Boundary conditions for parametric studies for U-shaped behavior for various nozzle length.

Fuel inlet velocity U_0 [m/s]	Nozzle length L_{res} [m]
5	0.03 ~ 23

Table2. Boundary conditions for parametric studies for pyrolysis effects on the lifted flame characteristics.

4.1. U-shaped behavior for various nozzle length

Figures 14a and 14b respectively show H_L and T_{max} as a function of U_0 with varying L_{res}. The "U-shape" H_L behavior is observed for all L_{res} conditions, demonstrating that the decreasing H_L behavior at relatively-low U_0 conditions is primarily attributed to the pyrolysis of DME. In addition, the slope of decreasing/increasing H_L behavior is more sensitive to the increase of L_{res}, which is related to the different level of pyrolysis with the U_0 variation. Moreover, for a given U_0, non-monotonic liftoff height behavior is also observed with increasing L_{res}. For instance, H_L decreases as L_{res} is increased from 0.75 to 1.5 m. However, as L_{res} is increased from 1.5 to 3 m, H_L increases. This may be due to the pyrolysis effect. To understand this behavior, additional numerical simulations are performed to identify pyrolysis effect on the lifted flame's characteristics.

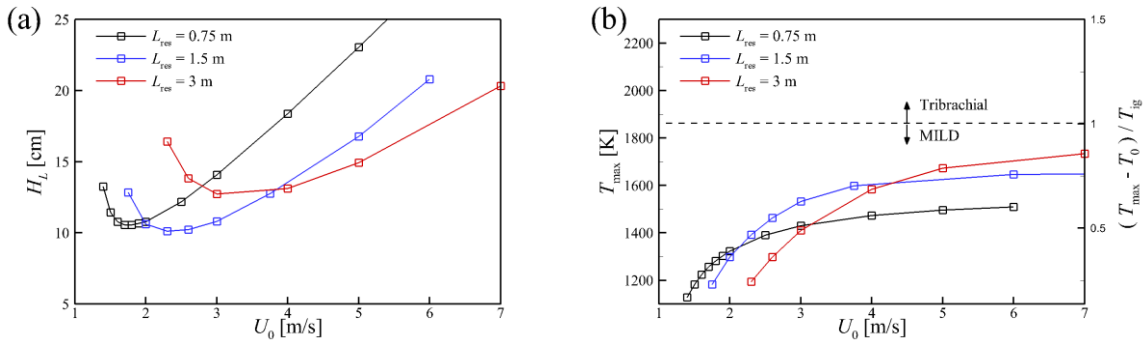

Figure 14. H_L (a) and (T_{max} - T_0) / T_{ig} (b) with different U_0 for autoignited laminar dimethyl ether jet flames under conditions (T_0 = 980 K, L_{res} = 0.75, 1.5, 3 m).

4.2. Pyrolysis effects on the lifted flame characteristics.

To identify the pyrolysis effect on the lifted flame, additional numerical simulations were performed by varying L_{res} from 3 cm to 23 m, while U_0 is fixed at 5 m/s. Figure 15 shows iso-contours of temperature and Y_{OH} for different L_{res}. As can be expected, the variation of H_L with increasing L_{res} shows a non-monotonic behavior. In addition, the flame structure is also changed with increasing L_{res}. For L_{res} = 0.75, 5, and 8 m cases in which the pyrolysis of DME proceeds slightly, the MILD combustion occurs. When a significant amount of DME is pyrolyzed, a tribrachial edge flame appears at L_{res} = 14 m and an attached flame occurs at L_{res} =17 m. Transition from the MILD combustion to the tribrachial edge flame occurs for L_{res} = 11 and 12.5 m. These results clearly show that the pyrolysis of DME affects not only the liftoff height but also the flame structure, and as such, we can conjecture that the autoignition characteristics of the lifted DME jet flames can also change depending on the degree of the pyrolysis of DME.

To quantitatively analyze the liftoff and flame structure characteristics, H_L and (T_{max} – T_0) / T_{ig} are shown in Fig. 16 as the function of L_{res}. (T_{max} – T_0) / T_{ig} repeats the increase and decrease behavior depending on the degree of pyrolysis and the transition occur as the amount of pyrolysis increase.

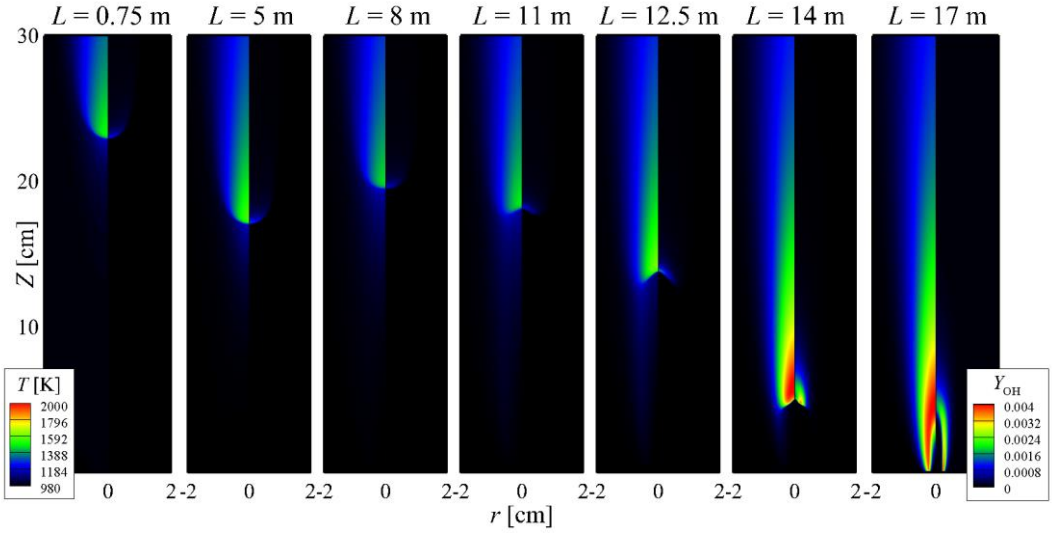

Figure 15. Iso-contours of (a) T (left half), and mass fraction of OH (right half) for autoignited laminar lifted DME jet flames under condition (L_{res} = 0.75 ~ 17 m with U_0 = 5m/s)

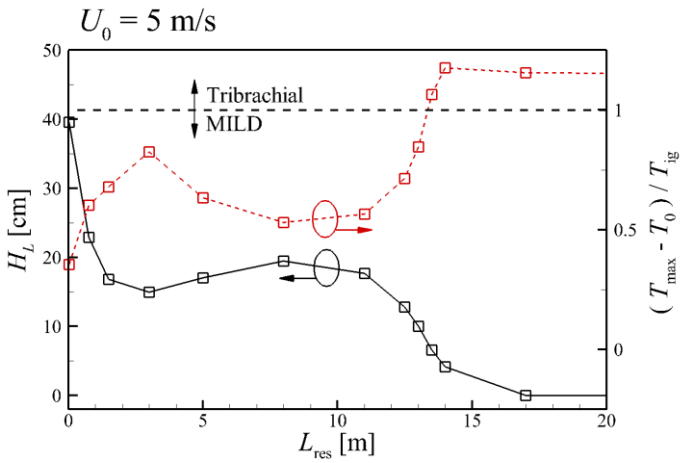

Figure 16. Variation of H_L and (T_{max} - T_0) / T_{ig} for different L_{res} under U_0 = 5 m/s condition

Since H_L of autoignited laminar lifted flame is highly affected by τ_{ig}^0, H_L and τ_{ig}^0 are shown in Fig. 17 as a function of L_{res}, where L_{res} is defined in 0-D domain as $L_{res} = U_0 \tau_{res}$. First, it is readily observed that τ_{ig}^0 variation with different level of pyrolysis also shows non-monotonic behavior. The flames in Fig. 17 can be classified into four different regimes based on their flame types: MILD combustion, transition, tribrachial edge flame, and attached flame regimes. In the MILD combustion regime (Regime I), τ_{ig}^0 well captures H_L behavior. This is because the inhomogeneity of ignition is low

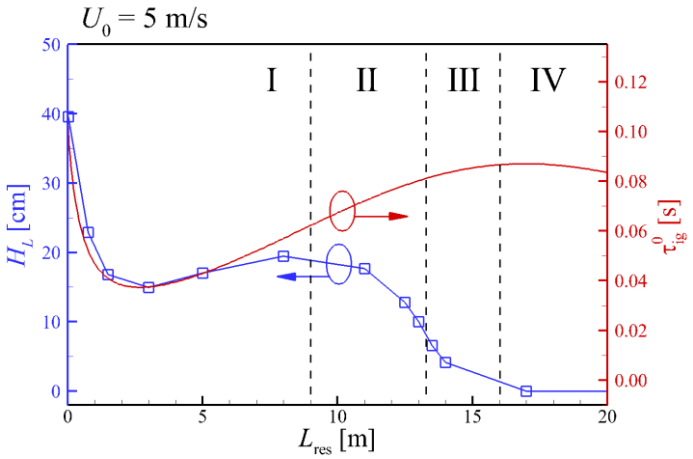

Figure 17. Variation of H_L and τ_{ig}^0 for different L_{res} under U_0 = 5 m/s condition

due to the small degree of DME pyrolysis. In the transition regime (Regime II), there is a slight difference between H_L and τ_{ig}^0. In the tribrachial edge flame regime (Regime III), τ_{ig}^0 does not capture H_L behavior. This is because the inhomogeneity of ignition is high due to the large degree of DME pyrolysis or ignition characteristic might be changed as the pyrolysis proceeds.

4.3. Ignition Characteristics in 2-D jet flame: CEMA

To investigate the flame characteristics for each regime, we investigate ignition characteristics of each regime by using CEMA. Figure 18 shows the isocontours of EI's for several important species in three kind of regimes (i.e., L_{res} = 1.5, 11, and 14 m cases, which represent the MILD combustion, transition, tribrachial edge flame regimes, respectively). The white dashed lines denote the flame regions defined by Re(λ_{exp}) = 0. Several points are noted from Fig. 18. First, hydrogen (Figs. 18a) does not participate in CEM for MILD combustion regime (i.e., L_{res} = 1.5 m) while these species are mainly contributed to CEM for the transition and tribrachial edge flame regimes (i.e., L_{res} = 11 and 14 m). On the other hand, the activation of HO_2 and H_2O_2 (Figs. 18d and 18e), which are important in the DME ignition as shown in 0-D calculation, is already finished upstream of the flame region for cases with L_{res} = 1.5 and 11 m, but it is not for L_{res} = 14 m. The resultant thermal ignition process shown in Fig. 18c shows the distinct difference between the MILD combustion and tribrachial edge flame regimes. For MILD combustion, thermal ignition activates after radical pool generation, but for tribrachial edge flame regime, thermal ignition activates from the very early stage of autoignition. In the MILD combustion regime, where the DME's pyrolysis does not proceed much, the overall ignition characteristics are dominated by the DME ignition. In the tribrachial edge flame regime, where the pyrolysis of DME proceeds significantly, the ignition characteristics behave more like hydrogen

ignition. To further identify different ignition characteristics for each regime, isocontours of PI's for several important reactions are shown in Figure 19.

Figures 19a ~ c show the PI isocontours of hydrogen related reactions: chain branching reaction of hydrogen, $H + O_2 \rightarrow O + OH$ (R1), the main heat release reaction of hydrogen, $H + OH \rightarrow H + H_2O$ (R3), and HO_2 formulation step, $H + O_2 + M \rightarrow HO_2 + M$ (R9), respectively. Figures 19d ~ f show the isocontours of PI's for DME related reactions. For the MILD combustion (i.e., L_{res} = 1.5 m), hydrogen related reactions do not affect the upstream of flamebase. Rather, these reactions are already diffused out from the flame region. Instead, DME reactions are activated upstream of the flamebase in the following sequence as already discussed above; after H-abstraction reactions of DME (Fig. 19d), CH_3OCH_3 + (OH, H, O, HO_2, O_2) → CH_3OCH_2 + (H_2O, H_2, OH, H_2O_2, HO_2), the important exothermic reaction of hydrocarbon (Fig. 19f), $H_2O_2 + M \rightarrow OH + OH + M$ (R16), subsequently occur near the flame region. Therefore, the ignition characteristics of the lifted flames in the MILD combustion regime follow the ignition of DME such that H_L variation can be well correlated with τ_{ig}^0. For the tribrachial edge flame regime (i.e., L_{res} = 14 m), on the other hand, DME ignition has nothing to do with the stabilization of flame base. Due to a large amount of H_2 generated from the pyrolysis, the ignition characteristics in this regime is dominated by the ignition of H_2 as demonstrated in Figs. 19a-c. In this regard, the H_L behavior for this regime is inconsistent with the variations of τ_{ig}^0. In summary, as the degree of pyrolysis increases, the autoignition characteristics of the DME jet change from those of DME to hydrogen. However, the liftoff height depends not only the characteristics of the ignition delay but also those of flame propagation. Therefore, to clearly understand the liftoff characteristics of the autoignited DME jet flames, further study using the flame speed and budget term analyses will be carried out as a future work.

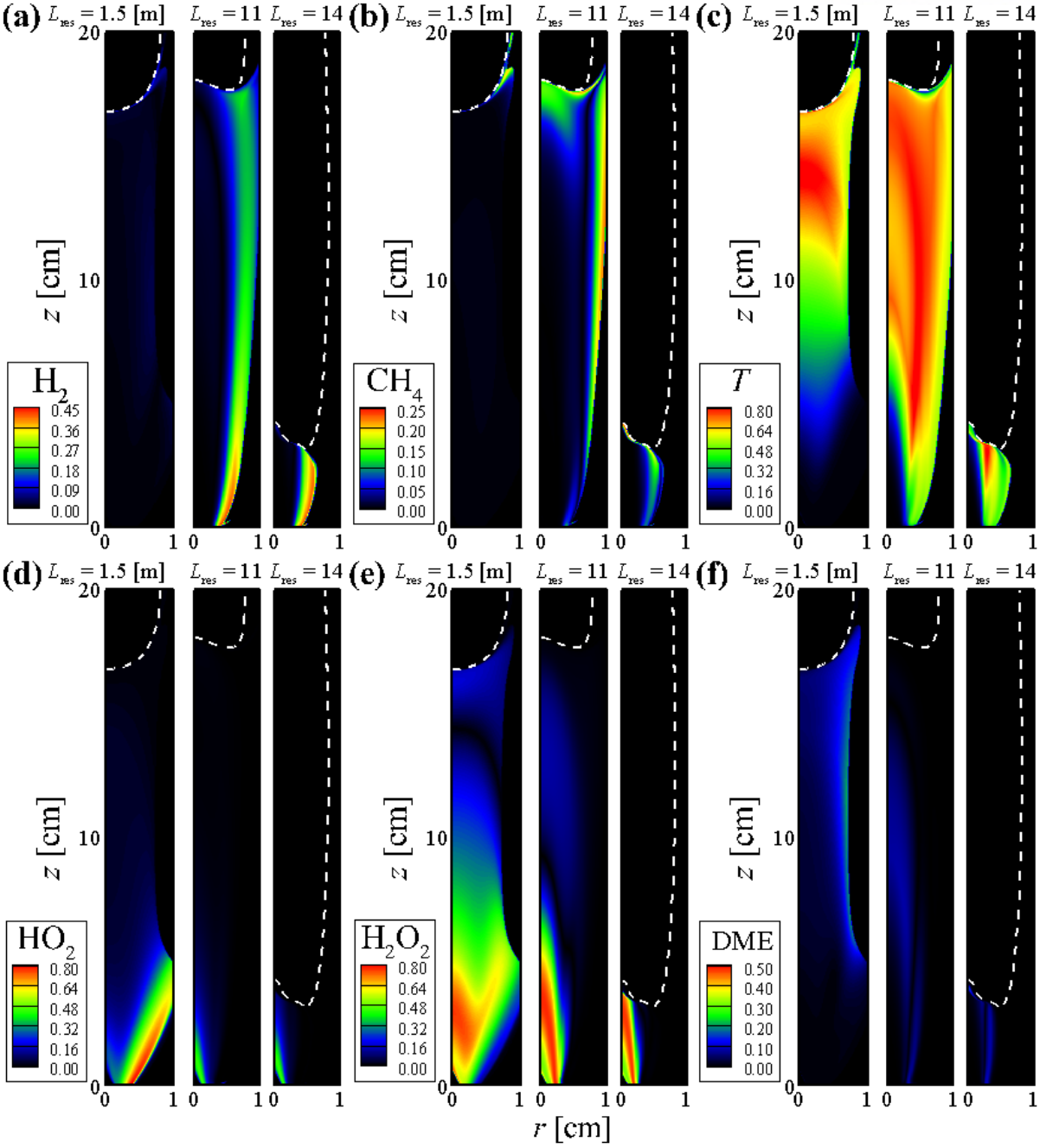

Figure 18. Isocontours of EI of (a) H_2, (b) CH_4, (c) T, (d) HO_2, (e) H_2O_2, and (f) DME for autoignited laminar lifted DME jet flames with different pyrolysis level, L_{res} = 1.5, 11, 14 m cases. The white dashed line represents an isoline of Re(λ_{exp}) = 0.

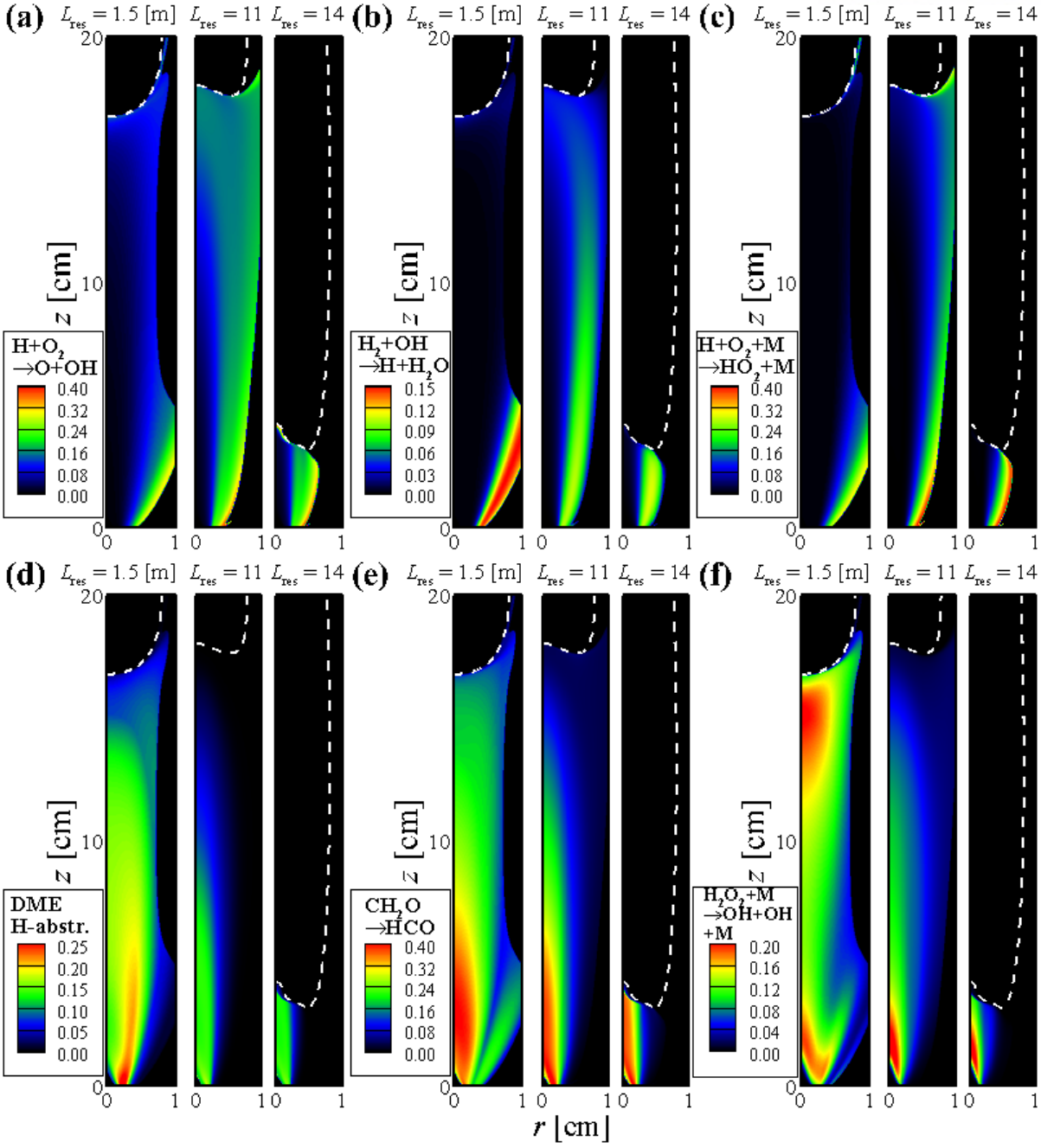

Figure 19. Isocontours of PI of (a) chain branching reaction of hydrogen, (b) heat release step of hydrogen, (c) HO_2 formulation, (d) DME H-abstraction, (e) CH_2O to HCO reactions, and (f) heat release step of hydrocarbon for autoignited laminar lifted DME jet flames with different pyrolysis level, L_{res} = 1.5, 11, 14 m cases. The white dashed line represents an isoline of Re(λ_{exp}) = 0.

5. Conclusions

The characteristics of autoignited laminar lifted dimethyl ether jet flames in heated coflow air were numerically investigated using the laminarSMOKE with a 53-species detailed chemical mechanism of dimethyl ether oxidation. The detailed numerical simulations were performed for various fuel jet velocities and fuel nozzle lengths. The numerical simulations can capture the 'U'-shaped liftoff height behavior, qualitatively similar to those observed in experiments. To identify the effect of inhomogeneity of ignition on the unusual H_L, additional numerical simulations with modified D_{H_2} were also carried out. The following results were obtained from the additional simulations.

1. From the simulations with different D_{H_2}, it was verified that the high diffusive characteristic of the hydrogen molecule is primarily attributed to differentiate the H_L from τ_{ig}^0 trend.

2. From 0-D simulation, it is verified that the longer the residence time is, the more CH_4 and H_2 are produced. In addition, DME autoignition is dominant at relatively-low pyrolysis stage and the overall flame characteristics change to hydrogen flame at relatively-high pyrolysis stage, based on the understanding of 0-D ignition characteristics.

3. From the CEMA, it was verified that the autoignition characteristics of lifted flame follow the ignition of DME such that H_L variations can be well correlated to τ_{ig}^0 under L_{res} = 0.75 m condition.

4. To elucidate the effect of pyrolysis, additional simulations were performed with L_{res} = 1.5 and 3 m. From results, the U-shaped liftoff height behavior is also observed similar to that at L_{res} = 0.75 m. The ignition of DME may be the attributed to the unusual behavior of the lifted flame at L_{res} = 1.5 and 3 m cases.

5. To further identify the pyrolysis effect on the lifted flame, additional numerical simulations were performed by changing L_{res} from 3 cm to 23 m. It is observed that for L_{res} = 5 and 8 m cases in which the pyrolysis proceeds slightly, the MILD combustion occurs. However, for L_{res} = 11 and 12.5 m cases in which the pyrolysis proceeds further, transition to the tribrachial edge flame occurs. When DME is further pyrolyzed, a tribrachial edge flame appears at L_{res} = 14 m and finally an attached flame occurs at L_{res} =17 m. Various flame structures are observed depending on the degree of pyrolysis.

6. Based on the flame structure and $(T_{max} - T_0) / T_{ig,}$ the flames can be classified into four different regimes. In the MILD combustion regime, τ_{ig}^0 well captures H_L behavior. At the tribrachial edge flame regime, τ_{ig}^0 does not capture H_L behavior.

7. From the CEMA, it was verified that in the MILD combustion regime, where pyrolysis does not proceed much, the overall ignition characteristics are dominated by the DME autoignition. In the tribrachial edge flame regime, where the pyrolysis of DME proceeds significantly, the ignition characteristics behave more like hydrogen flame.

References

[1] Y. Sato, "Development and Popularization of Heavy-Duty Vehicles Fueled by Dimethyl Ether (DME) as New Clean Alternative Energy," in *Proceedings of the 9th WSEAS International Conference on POWER SYSTEMS*.

[2] V. Golovitchev and J. Chomiak, "Evaluation of Ignition Improvers for Methane Autoignition," *Combust. Sci. Technol.,* vol. 135, pp. 31-47, 1998.

[3] Y. Tan, C. Fotache and C. K. Law, "Effects of NO on the ignition of hydrogen and hydrocarbons by heated counterflowing air," *Combust. Flame,* vol. 119, no. 3, pp. 346-355, 1999.

[4] Z. Chen, X. Qin, Y. Ju, Z. Zhao, M. Chaos and F. Dryer, "High temperature ignition and combustion enhancement by dimethyl ether addition to methane-air mixtures.," *Proc. Combust. Inst,* no. 31, pp. 1215-1222, 2007.

[5] X. Zheng, T. Lu, C. K. Law, C. K. Westbrook and H. J. Curran, "Experimental and computational study of nonpremixed ignition of dimethyl ether in counterflow," 2005.

[6] P. Dai, Z. Chen and S. Chen, "Ignition of methane with hydrogen and dimethyl ether addition," *Fuel,* vol. 118, pp. 1-8, 2014.

[7] C. Arounmanis, C. Bae, R. Crookes and E. Kinoshita, "The potential of di-methyl ether (DME) as an alternative fuel for compression-ignition engines: a review," *Fuel,* vol. 87, pp. 1014-1030, 2008.

[8] Y. Hidaka, K. Sato and M. Yamane, "High-temperature pyrolysis of dimethyl ether in shock waves," *Combust. Flame,* vol. 123, pp. 1-22, 2000.

[9] B. C. Choi, K. N. Kim and S. H. Chung, "Autoignited laminar lifted flames of propane in coflow jets with tribrachial edge and mild combustion," *Combust. Flame,* vol. 156, pp. 396-404, 2009.

[10] B. C. Choi and S. H. Chung, "Autoignited laminar lifted flames of methane, ethylene, ethane, and n-butane jets in coflow air with elevated temperature," *Combust. Flame,* vol. 157, pp. 2348-2356, 2010.

[11] B. C. Choi and S. H. Chung, "Autoignited laminar lifted flames of methane/hydrogen mixtures in heated coflow air," *Combust. Flame,* vol. 159, pp. 1481-1488, 2012.

[12] S. K. Choi and S. H. Chung, "Autoignited and non-autoignited lifted flames of pre-vaporized n-heptane in coflow jets at elevated temperatures," *Combust. Flame,* vol. 160, pp. 1717-1724, 2013.

[13] S. K. Choi, S. Al-Noman and S. H. Chung, "Simulation of non-autoignited and autoignited laminar non-premixed jet flames of syngas in heated coflow air," *Combust. Sci. Technol.,* vol. 187, pp. 132-147, 2015.

[14] S. M. Al-Noman, S. K. Choi and S. H. Chung, "Autoignition characteristics of laminar lifted jet flames of pre-vaporized iso-octane in heated coflow air," *Fuel,* vol. 162, pp. 171-178, 2015.

[15] S. M. Al-Noman, S. K. Choi and S. H. Chung, "Numerical study of laminar non-premixed methane flames in coflow jets: Autoignited lifted flames with tribrachial edges and mild combustion at elevated temperatures," *Combust. Flame,* vol. 171, pp. 119-132, 2016.

[16] S. H. Chung and B. J. Lee, "On the characteristics of laminar lifted flames in a non-premixed jet," *Combust. Flame,* vol. 86, pp. 62-72, 1991.

[17] B. J. Lee and S. H. Chung, "Stabilization of lifted tribrachial flames in a laminar non-premixed jet," *Combust. Flame,* vol. 109, pp. 163-172, 1997.

[18] S. Al-Noman and S. Chung, "Autoignited lifted flame of dimethyl ether in heated coflow air," *Combust. Flame,* vol. 195, pp. 75-83, 2018.

[19] K. S. Jung, S. O. Kim, T. Lu, S. H. Chung, B. J. Lee and C. S. Yoo, "Differential diffusion effect

on the stabilization characteristics of autoignited laminar lifted methane/hydrogen jet flames in heated coflow air," *Combust. Flame,* vol. 198, pp. 305-319, 2018.

[20] H. G.Weller, G. Tabor, H. Jasak and C. Fureby, "A tensorial approach to computational continuum mechasnics using object-oriented techniques," *Comput. Phys,* vol. 12, pp. 620-631, 1998.

[21] R. Hall, "The radiative source term for plane-parallel layers of reacting combustion gases," *J. Quant. Spectrosc. Radiat. Transf.,* vol. 49, pp. 517-523, 1993.

[22] A. Cuoci, A. Frassoldati, T. Faravelli and E. Ranzi, "A computational tool for the detailed kinetic modeling of laminar flames: application to C2H4/CH4 coflow flames," *Combust. Flame,* vol. 160, pp. 870-886, 2013.

[23] A. Cuoci, A. Frassoldati, T. Faravelli and E. Ranzi, "Numerical modeling of laminar flames with detailed kinetics based on the operator-splitting method," *Energy Fuels,* vol. 27, pp. 7730-7753, 2013.

[24] Z. Zhao, M. Chaos, A. Kazakov and F. L. Dryer, "Thermal decomposition reaction and a comprehensive kinetic model of dimethyl ether," *Int. J. Chem. Kinet.,* vol. 40, no. Int J Chem Kinet, pp. 1-18, 2008.

[25] C. S. Yoo, T. Lu, J. H. Chen and C. K. Law, "Direct numerical simulations of ignition of a lean n-heptane/air mixture with temperature inhomogeneities at constant volume: Parametric study," *Combust. Flame,* vol. 158, pp. 1727-1741, 2011.

[26] M. B. Luong, G. H. Yu, T. Lu, S. H. Chung and C. S. Yoo, "Direct numerical simulations of ignition of a lean n-heptane/air mixture with temperature and composition inhomogeneities relevant to HCCI and SCCI combustion," *Combust. Flame,* vol. 162, pp. 4566-4585, 2015.

[27] T. Lu, C. S. Yoo, J. H. Chen and C. K. Law, "Three-dimensional direct numerical simulation of a turbulent lifted hydrogen jet flame in heated coflow: a chemical explosive mode analysis," *J. Fluid Mech,* vol. 652, pp. 45-64, 2010.

[28] Z. Luo, C. S. Yoo, E. S. Richardson, J. H. Chen, C. K. Law and T. Lu, "Chemical explosive mode analysis for a turbulent lifted ethylene jet flame in highly-heated coflow," *Combust. Flame,* vol. 159, pp. 265-274, 2012.

[29] R. Shan, C. S. Yoo, J. H. Chen and T. Lu, "Computational diagnostics for n-heptane flames with chemical explosive mode analysis," *Combust. Flame,* vol. 159, pp. 3119-3127, 2012.

[30] M. B. Luong, G. H. Yu, S. H. Chung and C. S. Yoo, "Ignition of a lean PRF/air mixture under RCCI/SCCI conditions: Chemical aspects," *Proc. Combust. Inst.,* vol. 36, pp. 3587-3596, 2017.

[31] M. d. Joannon, A. Saponaro and A. Cavaliere, "Zero-dimensional analysis of methane diluted oxidation in rich conditions," *Proc. Combust. Inst.,* vol. 28, pp. 1639-1646, 2000.

[32] A. Cavaliere and M. d. Joannon, "Mild combustion," *Prog. Energy Combust. Sci.,* vol. 30, pp. 329-366, 2004.

[33] R. Kee, F. Rupley, E. Meeks and J. Miller, "CHEMKIN-III: a fortran chemical kinetics package for the analysis of gas-phase chemical and plama kinetics," *SAND96-8216.*

Acknowledgments

I would like to express my special thanks of gratitude to my research advisor, Professor Chun Sang Yoo for the continuous encouragement and guiding. I have learned a lot in this laboratory.

I am also grateful to my research partner Ki Sung Jung who supported me, and I am thank my parents for the unceasing encouragement, support and attention.